Neuron, Vol. 28, 205–220, October, 2000, Copyright ©2000 by Cell Press

Quantal Release of Serotonin

Dieter Bruns,*‡ Dietmar Riedel,*
Jürgen Klingauf,† and Reinhard Jahn*
Max-Planck Institute for Biophysical Chemistry
*Department of Neurobiology and
†Department of Membrane Biophysics
Am Fassberg 11
D-37077 Göttingen
Germany

Summary

We have studied the origin of quantal variability for small synaptic vesicles (SSVs) and large dense-cored vesicles (LDCVs). As a model, we used serotonergic Retzius neurons of leech that allow for combined amperometrical and morphological analyses of quantal transmitter release. We find that the transmitter amount released by a SSV varies proportionally to the volume of the vesicle, suggesting that serotonin is stored at a constant intravesicular concentration and is completely discharged during exocytosis. Transmitter discharge from LDCVs shows a higher degree of variability than is expected from their size distribution, and bulk release from LDCVs is slower than release from SSVs. On average, differences in the transmitter amount released from SSVs and LDCVs are proportional to the size differences of the organelles, suggesting that transmitter is stored at similar concentrations in SSVs and LDCVs.

Introduction

The vesicle hypothesis of chemical transmission proposes that neurotransmitter is discharged in multimolecular packets from synaptic vesicles. In most central neurons, the postsynaptic response to such a single packet of neurotransmitter shows wide variations in amplitude (Bekkers et al., 1990; Raastad et al., 1992; Liu et al., 1999). Despite intensive research, the origin of quantal variability has remained controversial (Redman, 1990; Korn and Faber, 1991; Stevens, 1993; Frerking and Wilson, 1996). Evidence has been presented that quantal response is limited by the availability of postsynaptic receptors (Edwards et al., 1990; Tang et al., 1994; Tong and Jahr, 1994; Auger and Marty, 1997), suggesting that transmitter concentrations in the synaptic cleft are generally sufficient to produce saturation of the affected receptor population. Other studies suggested, rather, that quantal variability is due to variations in the amount of released transmitter producing nonsaturating concentrations of transmitter in the synaptic cleft (Frerking et al., 1995; Silver et al., 1996; Liu et al., 1999). Thus, quantal variability at synapses in the CNS can be dominated either by pre- or postsynaptic mechanisms, depending on the preparation under study.

‡To whom correspondence should be addressed (e-mail: dbruns@mpibpc.gwdg.de).

Major advances in the understanding of presynaptic mechanisms are hampered by the necessity to record postsynaptic responses in order to infer presynaptic events. To overcome this limitation, we used carbon fibers as electrochemical detectors that allow us to measure the amount of neurotransmitter released by a vesicle directly. As a model system, we have chosen Retzius cells that represent large serotonergic neurons and that can be readily isolated from the CNS of the leech (*Hirudo medicinalis*). These neurons retain their capability to synthesize, store, and release 5-HT when they are grown in isolation (Henderson, 1983). In a previous study (Bruns and Jahn, 1995), we adapted amperometric recordings to monitor serotonin release from individual Retzius neurons in culture. We characterized distinct classes of amperometric signals that are due to exocytosis of SSVs and LDCVs present in these neurons.

Here, we have explored the question to what extent variations in quantal transmitter release from both the SSVs and the LDCVs are related to the size variability of the corresponding secretory organelle. For this, we used a combination of electron microscopy and carbon fiber amperometry. It will be shown that SSVs and LDCVs exhibit a differential subcellular distribution between the axon and the soma. In close correlation, we observe a distinct pattern of amperometric signals at axonal and somatic recording sites that parallels the subcellular distribution of SSVs and LDCVs between these cellular regions. On average, the differences in quantal size observed for SSV and LDCV exocytosis correlate well with the size differences of the secretory organelles. The amount of transmitter released from a SSV varies proportionally to the volume of the vesicle, whereas transmitter discharge from LDCVs shows a higher degree of variability than expected from its size distribution.

Results

SSVs and LDCVs Are Differentially Distributed between Axon and Soma

The typical ultrastructural features of a cultured Retzius cell are shown in Figure 1. A survey of the axon and the soma reveals that clusters of SSVs (arrowheads) are exclusively found in the axon, whereas LDCVs are present at both cellular regions (compare Figures 1A and 1E). It should be noted that the axon stump consists of a central cylinder that sends out lateral arborizations forming a condensed network of axonal endings (data not shown). Many axonal extensions that contain clusters of SSVs are found on the surface of the axon stump, making them directly accessible to carbon fiber amperometry (Figures 1A–1D). Within such terminal regions, SSVs are clustered directly opposing the plasma membrane. LDCVs often surround those clusters but are also found scattered throughout the cytoplasm. Morphological structures that resemble closely these putative release sites have been seen in junctions formed between presynaptic Retzius cells and postsynaptic P cells (Kuffler et al., 1987). Occasionally, axon terminals exhibit active zone–like thickenings (electron-dense bars) to which rows of SSVs in direct contact with the plasma

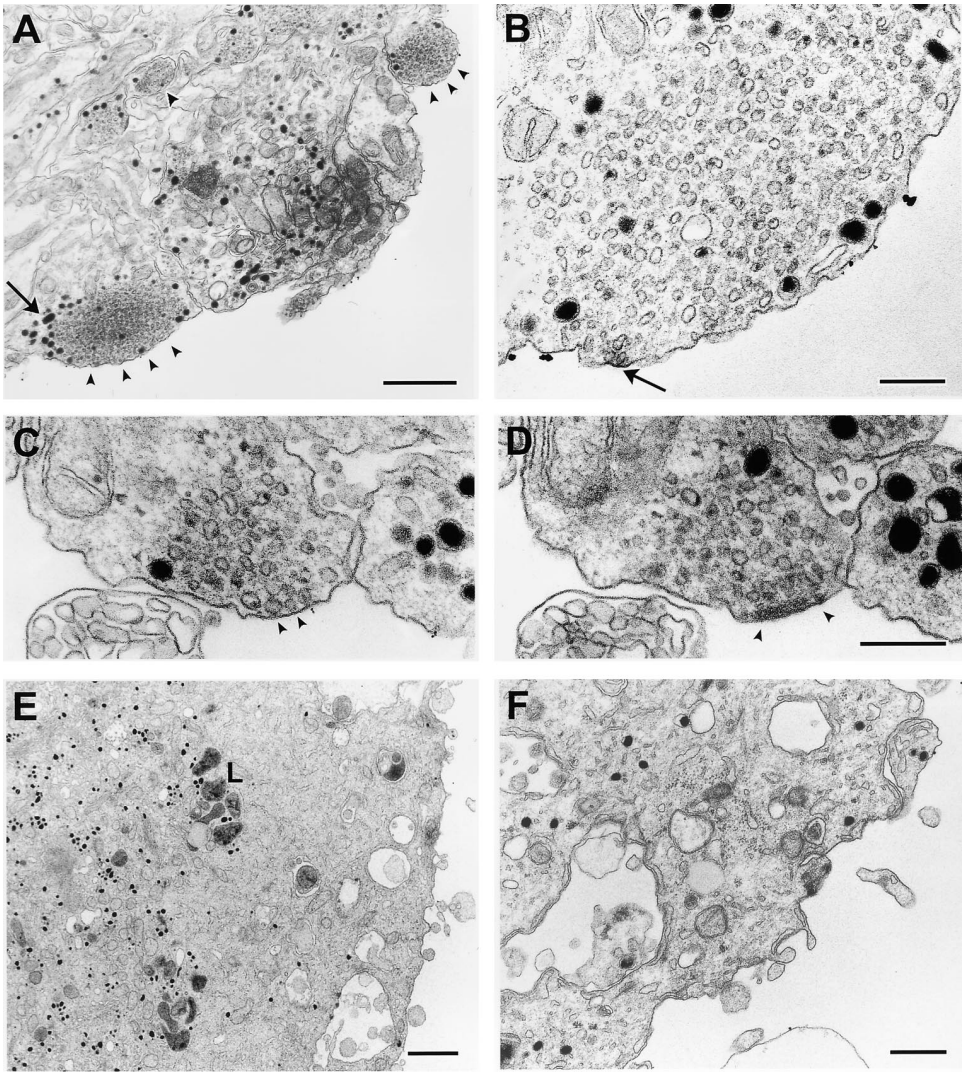

Figure 1. Subcellular Distribution of SSVs and LDCVs in Retzius Cells

(A) Electron micrograph depicting several clusters of SSVs located at superficial and underlying structures (arrowheads) at the tip of the axon. Note the less tightly clustered distribution of LDCVs (arrow). LDCVs often surround SSV clusters in a capped arrangement. Scale, 1 μm.

(B) Sample cluster of SSVs at high magnification. SSVs outnumber LDCVs within an axon terminal. Some SSVs (arrow) are immediately adjacent to the plasma membrane. It should be noted that several SSV profiles can be seen to be partially filled with electron-dense material following sequential glutaraldehyde-osmium fixation. The osmiophilic product likely results from a direct oxidation of 5-HT or its aminergic analogs within their storage sites (Tranzer and Thoenen, 1967; Hökfelt, 1968; Arluison and de la Manche; 1980; Fried et al., 1981). Further experiments will address this finding in more detail (see below). Scale, 250 nm.

(C and D) Two consecutive sections (thickness, 80 nm). SSVs are found in direct contact with the plasma membrane (arrowheads) and in close apposition with a presynaptic dense bar indicating an active zone ([D], flanked by arrowheads). Scale, 250 nm.

(E) Survey of the soma of a Retzius cell. LDCVs are concentrated in perinuclear regions (left side) that are enriched with Golgi complexes and lysosomes (L). The concentric orientation of LDCVs around the nucleus and their sparse distribution at the somatic periphery agrees with the distribution pattern of LDCVs in vivo (Rude et al., 1969). Scale, 1 μm.

(F) Only a few LDCVs are observed in the vicinity of the somatic plasma membrane. Scale, 500 nm.

membrane are aligned (see consecutive sections in Figures 1C and 1D). Evidently, morphological specializations characteristic of mature release sites are maintained when Retzius cells grow in isolation. In general, the spatial organization of SSVs and LDCVs provides a picture that is strikingly similar to those seen at serotonergic synapses in the vertebrate CNS (Beaudet and Descarries, 1981; Chazal and Ralston, 1987; Moukhles et al., 1997). While both LDCVs and SSVs are found at axonal sites, the somata of the neurons contain only LDCVs. Here, these vesicles are concentrated in perinuclear regions enriched with prominent Golgi complexes and endoplasmic reticulum (Figure 1E). The density of the LDCVs decreases toward the plasma membrane, and only a few granules were observed in its direct vicinity (Figure 1F). A similar distribution pattern of LDCVs has been observed in these neurons in situ (Rude et al., 1969).

Morphometric Analysis of Secretory Organelles

On electron micrographs, obtained with a carefully calibrated microscope, we determined the cross-sectional

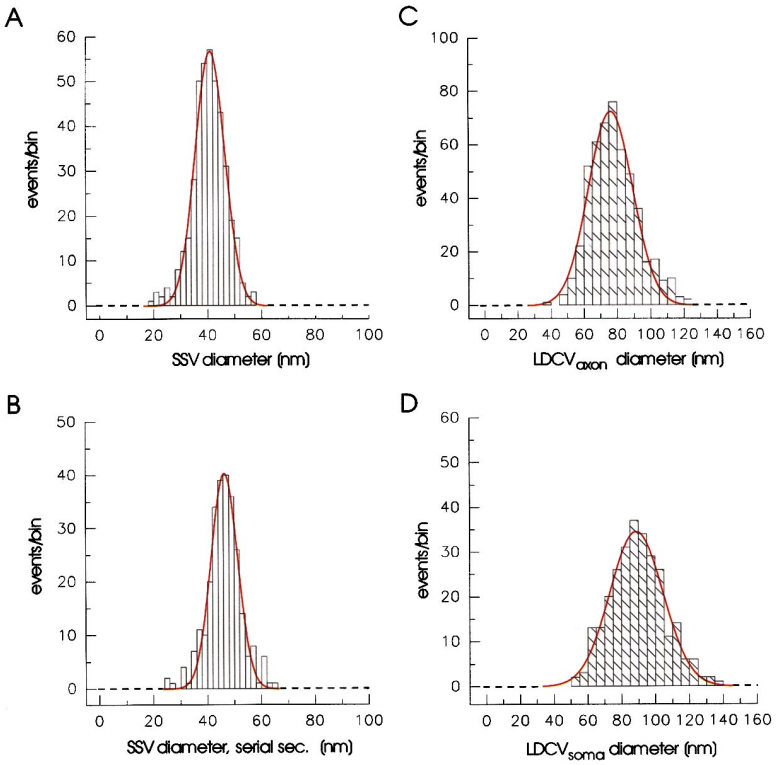

Figure 2. Sizes of SSVs and LDCVs in Retzius Cells

Distribution of SSV diameters ([A], n = 404) and LDCV diameters at axonal ([C], n = 494) and somatic ([D], n = 276) sites. (B) Size distribution of SSVs entirely contained within an 80 nm section (as judged from serial sections, n = 270; 2 cells, 8 section series). The red curve fitted to each of the distributions (A–D) is a Gaussian with the parameters indicated in Table 1. Data of (A), (C), and (D) collected from 4 cells.

diameters of the different vesicle types (see Experimental Procedures). The SSV profiles have a mean diameter of 40.9 ± 5.5 nm (Figure 2A). The size distribution of SSVs closely resembles that observed in other preparations (Palay and Chan-Palay, 1974; Bekkers et al., 1990; Zhang et al., 1998). The average diameter of LDCVs in the axon is 76.0 ± 13.3 nm, about two times larger than that of SSVs. LDCVs in the soma have a mean diameter of 88.7 ± 15.8 nm and are significantly larger than their axonal counterparts (Student's t test, $p < 0.001$; Figures 2C and 2D). The different diameters of somatic and axonal LDCVs calculate to a nearly 1.6-fold larger volume of somatic LDCVs. The mean diameters corrected for a section thickness of 50 nm (Parsons et al., 1995) are given in Table 1. We also determined the mean outer diameter of SSVs that are entirely contained within an 80 nm section, as judged from examination of serial sections (Figure 2B). The latter approach revealed a slightly narrower size distribution of SSV profiles. Their average (46.3 ± 4.9 nm) agrees with the calculated diameter, showing that the correction procedure renders an accurate estimate of vesicle size in our experiments. The size variability of the secretory organelles is reasonably well approximated with Gaussian distributions, agreeing with reports in other preparations (Bekkers et al., 1990; Lagnado et al., 1996; Lenzi et al., 1999; Plattner et al., 1997).

Table 1. Diameters of SSVs and LDCVs in Serotonergic Retzius Cells

Vesicle Type	Number of Profiles	Diameter (nm)	Corrected Diameter (nm)
SSV	404	40.9 ± 5.5	45.6
SSV^2	270	46.3 ± 4.95	—
LDCV-Axon	494	76.0 ± 13.3	88.1
LDCV-Soma	276	88.7 ± 15.8	103.7

Measurements are given as mean ± SD. Diameters are obtained from the Gaussian fits shown in Figure 2 and are corrected for section thickness (50 nm) according to Parsons et al. (1995). SSV^2, mean diameter of SSVs that are entirely contained within an 80 nm section.

SSVs Serve as Aminergic Storage Organelles

A large number of different experimental approaches have firmly established the aminergic character of Retzius cells (Rude et al., 1969; McAdoo and Coggeshall, 1976; Lent et al., 1979; Henderson, 1983). These studies suggested that serotonin is the major, if not the only, classical transmitter contained in these neurons. Immunoelectron microscopy demonstrated that serotonin is present in dense-cored vesicles (Kuffler et al., 1987). The fixation protocol used to preserve antigenecity did not allow for preservation of SSVs. Here, we employed permanganate as a fixative to show that SSVs serve as aminergic storage organelles. Permanganate reacts specifically with biogenic amines, forming an electron-dense precipitate within aminergic but not within other types of storage organelles (e.g., cholinergic; Hökfelt and Jonsson, 1968; Klein et al., 1982; Thureson-Klein, 1983).

In fact, an electron-dense precipitate is frequently observed in SSVs when Retzius cells are fixed with permanganate (Figure 3A). A similar reaction product is seen when en bloc staining with uranyl acetate is omitted, indicating that the precipitate depends on permanganate (data not shown). Cholinergic AE motonerons (Sargent, 1977), isolated from the CNS of the leech, were cultured and processed in parallel to serve as controls. As expected, all SSV profiles seen in these neurons remain electronlucent (Figure 3B). These results suggest that electron opacity of SSVs in Retzius cells is related to their amine content.

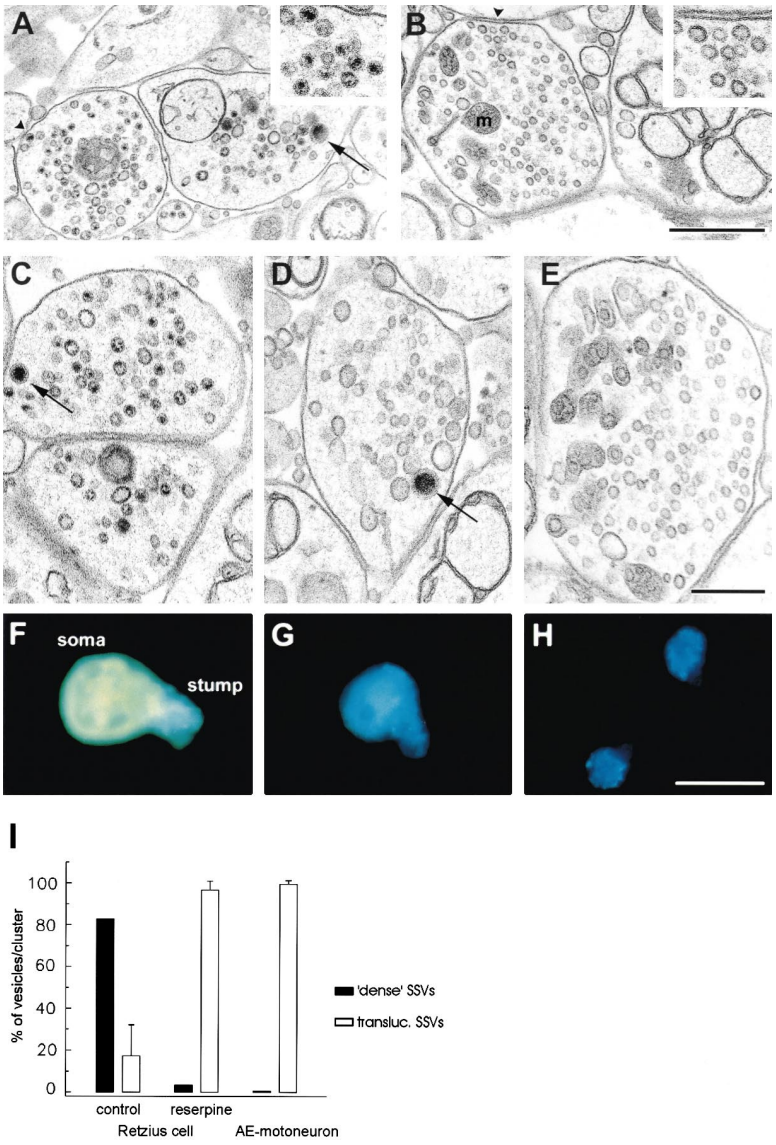

Figure 3. SSVs Serve as Aminergic Storage Organelles in Retzius Cells

(A) SSVs in Retzius cells contain electron-dense cores of varying size after fixation in permanganate. A few LDCVs (arrow) are also present.

(B) SSVs found in the axon of cholinergic AE motoneurons remain translucent when fixed with permanganate. m, multivesicular body. Scale (A and B), 500 nm. Insets, double magnification of the indicated regions (arrowheads) in (A) and (B).

(C–E) Electron-dense cores frequently seen in SSVs of control Retzius cells (C) are absent in SSV profiles of reserpine-treated Retzius cells (D) or AE motoneurons (E). Electron density of LDCVs (arrows) is unchanged after reserpine treatment. Scale (C–E), 250 nm.

(F–H) Effects of reserpine on the serotonin content of Retzius cells shown by fluorescence micrographs of cells processed in parallel to our electron microscopy shown in (C)–(E). Staining of control Retzius cells (F) by glyoxylic acid technique produced a 5-HT-specific fluorescence in the soma and the stump of the Retzius cell that is strongly reduced in reserpine-treated Retzius cells (G) and absent from AE motoneurons ([H], 2 motoneurons shown). Staining with glyoxylic acid was performed using the technique described by Dietzel and Gottmann (1988). Fluorescence was viewed with filter combination BP 400, FT 460, LP 470 under a Zeiss fluorescence microscope using a mercury vapor lamp. Scale (F–H), 60 μm.

(I) Percentage of electrondense SSV profiles per vesicle cluster observed in Retzius cells (control: 3 cells, 32 clusters, 680 vesicles; reserpine treated: 3 cells, 34 clusters, 660 vesicles) and AE motoneurons (3 cells, 17 clusters, 590 vesicles).

To verify this observation, Retzius cells were cultured for 2 days in the presence of 1 μM reserpine, an inhibitor of vesicular monoamine uptake. This treatment reduces greatly the occurrence of electron-dense precipitates in SSVs (compare Figures 3C and 3D). On average, the proportion of electron-dense SSV profiles per cluster decreases about 15-fold from 84% in control cells to 5% in reserpine-treated neurons (Figure 3I). Transmitter depletion is verified by staining Retzius cells with the glyoxylic acid technique (Torre and Surgeon, 1976), which revealed less serotonin-specific fluorescence in reserpine-treated Retzius cells than in untreated cells (Figures 3F and 3G). These results are consistent with our previous observation showing that reserpine treatment abolishes synaptic signaling between Retzius and P cells (Bruns et al., 1993). In contrast to SSVs, LDCVs maintained their electron-dense content after reserpine treatment. This result agrees with reports of similar studies on sympathetic nerve cells, suggesting that factors other than amine transmitter content are responsible for the electron density of LDCVs (Till and Banks, 1976; Fried et al., 1981). Taken together, the results indicate that in Retzius neurons SSVs serve, in addition to LDCVs (Kuffler et al., 1987), as aminergic storage organelles.

Quantal Release at Axonal Sites

Exocytosis of SSVs occurs more frequently and more rapidly than exocytosis of LDCVs when Retzius cells are stimulated with single action potentials (Bruns and Jahn, 1995). This observation may be a consequence of the different spatial organization of the vesicle types within the axon terminal, as shown in Figure 1. To facilitate the stimulation of both SSV and LDCV exocytosis, we applied the Ca^{2+} ionophore ionomycin, which should cause a long-lasting and spatially uniform intracellular Ca^{2+} rise. Viability of the neurons, as judged from a normal resting potential (50–60 mV) and action potential wave forms, was verified in all experiments by recording the actual membrane potential with an additional microelectrode. In the first set of our experiments, the tip of a carbon fiber was manipulated to the distal end of the

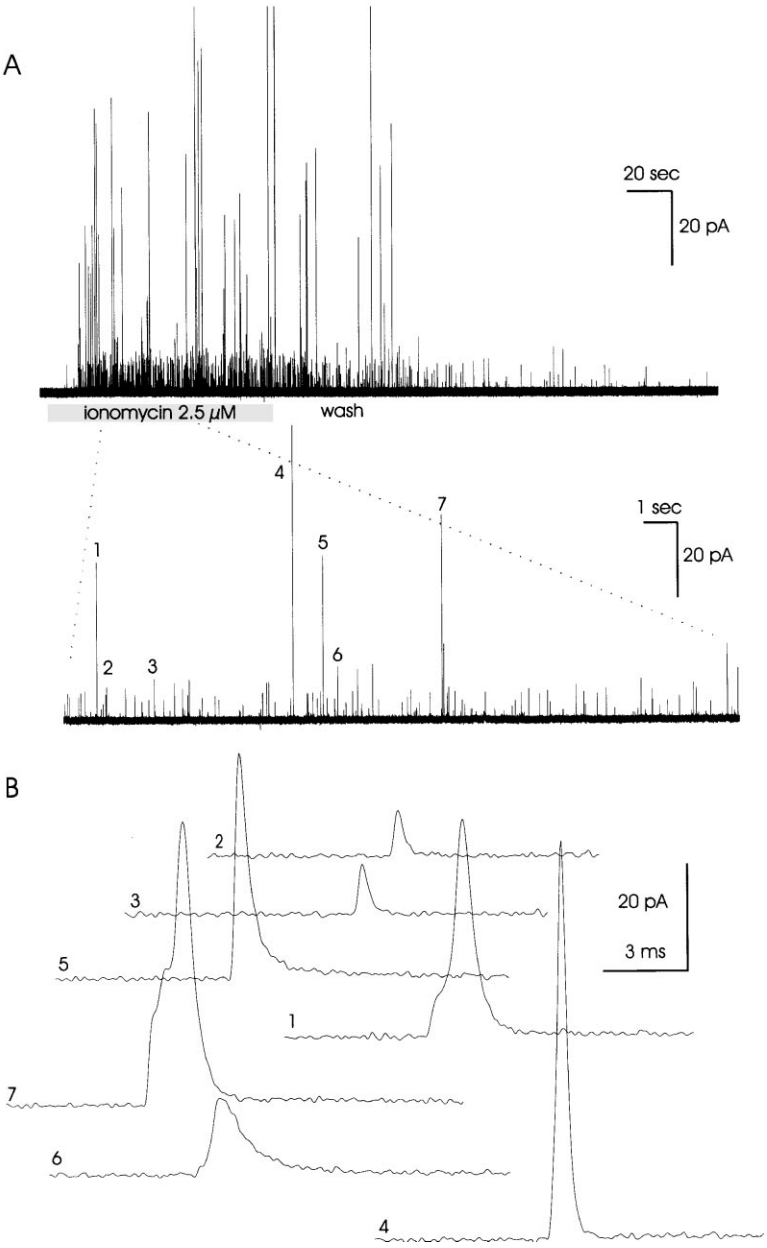

Figure 4. Amperometric Events Evoked by Ionomycin at the Axon of a Retzius Cell

(A) Superfusion of the cell with ionomycin (2.5 μM; bar) triggers a strong increase in the frequency of amperometric spikes that progressively returns to baseline levels (0.02–0.05 Hz) upon superfusion with Ringer's solution (wash). The mean frequency of events is about 4.3 Hz between 15 and 150 s after onset of ionomycin application. The extended time scale shows that amperometric signals are resolved as discrete spikes. Application of the ionophore did not change the resting membrane potential (data not shown) measured with an additional microelectrode.

(B) Transient oxidation currents taken from the recording in (A) as indicated with corresponding numbering in the extended trace. Traces (2) and (3) show small and rapid current transients that comprise the majority of exocytotic events in this recording and that are due to transmitter release from single SSVs. LDCV fusion events (as judged from their large quantal size, traces [1] and [4]–[7]) are often preceded by a "foot" signal that arises presumably from leakage of transmitter through a slowly dilating fusion pore.

axon stump of a single Retzius cell. The carbon fiber was brought into direct contact with the plasma membrane in order to minimize diffusional loss of released transmitter and temporal distortion of the transmitter signal. Superfusion of the neuron with Ringer's solution containing 2.5 μM ionomycin causes, after variable delays of 2–10 s, a strong increase in the frequency of amperometric spikes (Figure 4A). In the presence of the ionophore, exocytosis proceeds at a rather constant rate (3.1 ± 1.9 events/s, n = 12) and slowly declines to baseline levels when ionomycin is removed by continuous washing with Ringer's solution. As shown in Figure 4, oxidative current transients can be resolved as discrete events even at times of high activity. In agreement with our morphological observations, the evoked response is comprised of exocytotic events that differ with respect to their charge and amplitude. We observed small and rapid events as well as significantly larger events with a more variable time course that are likely due to transmitter release from SSVs and LDCVs, respectively. The charge distribution, derived from the integral of the oxidative current spikes in 12 cells, shows a strong peak at small values of about 3 fC and a significant fraction of larger responses (Figure 5A). Consistent with our previous observations (Bruns and Jahn, 1995), charge values are broadly spread in a skewed, non-Gaussian distribution. If the molecular mechanism for loading of transmitter into the vesicles operates until a limiting concentration is achieved, then the amount of transmitter stored in a vesicle should vary with the cube of the vesicle diameter. A cubic root transformation of the charges reveals an obvious bimodal distribution (Figure 5B) that is well approximated with two Gaussian distributions, as expected for transmitter release from differentially sized vesicle popula-

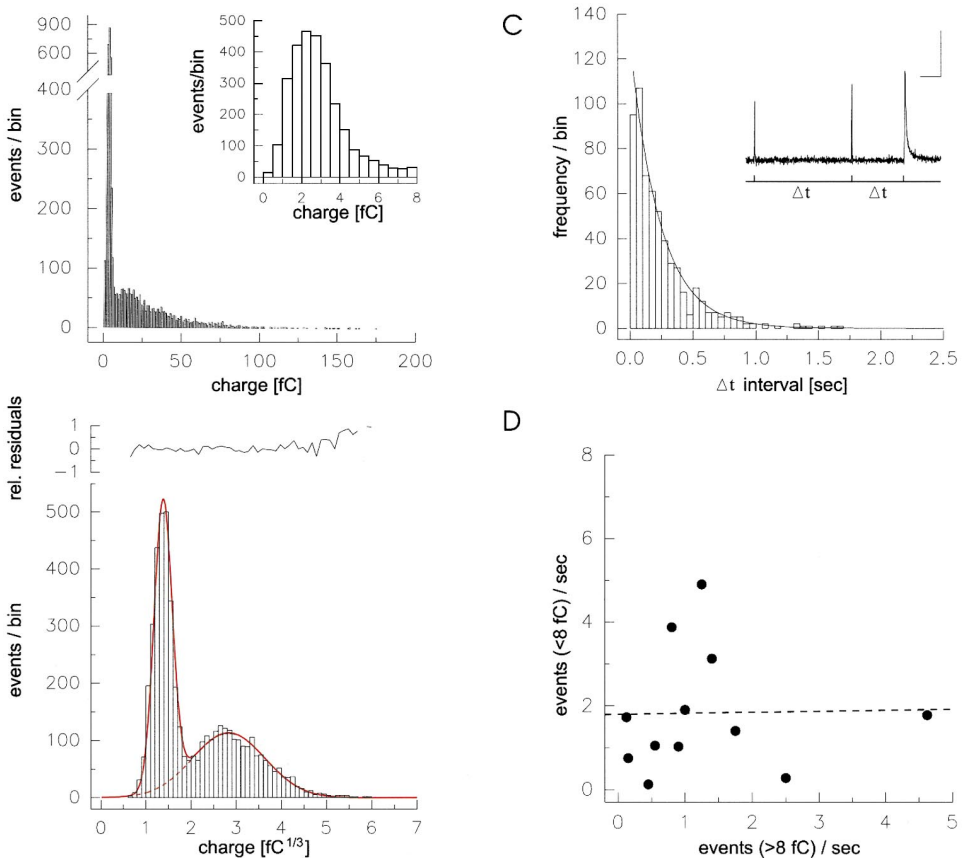

Figure 5. Characteristics of Amperometric Signals at Axonal Recording Sites

(A) Charge distribution derived from the time integral of transient oxidation currents stimulated by ionomycin. The bimodal distribution has its peak between 2 and 4 fC and shows a significant "tail" of large event responses ranging up to 150 fC. Data were collected from 12 cells (4738 events; bin width, 1.0 fC). Inset, charge distribution of the small events (0.2–8.0 fC) shown at a bin width of 0.5 fC.

(B) Frequency distribution of the cube-rooted amperometric spike charge of the data shown in (A). The distribution is well approximated by the sum of two Gaussian distributions (continuous red curve) with the following parameters: $N_{small} = 2472$ events, $mean_{small} = 1.36\ fC^{1/3}$, $CV_{small} = 0.15$; $N_{large} = 2244$, $mean_{large} = 2.82\ fC^{1/3}$, $CV_{large} = 0.29$. The Gaussian fit provides an adequate description of the data over the entire range of charges as judged from the relative residuals plotted on top of (B). Dashed red curve: extrapolation of the right-hand Gaussian fit showing the presumptive contribution of the larger event type to the data range <8 fC.

(C) Distribution of latency times (Δt) between successive events (measured as shown in the inset; scaling: 25 ms, 5 pA). The solid line represents an exponential probability density function: $f(t) = \tau^{-1}e^{-t/\tau}$ multiplied with the total number of observations ($n = 607$) and the bin width (50 ms).

(D) Plot of the mean frequency of small events (<8.0 fC) against the mean frequency of large events (>8.0 fC) measured between 40 and 80 s after the onset of ionomycin application. Data are collected from 12 cells. A linear regression is fitted to the data (dashed line).

tions. The cube-rooted quantal size of the larger events ($2.82 \pm 0.81\ fC^{1/3}$) is, on average, about 2-fold larger than that of the smaller event type ($1.36 \pm 0.2\ fC^{1/3}$).

An alternative interpretation of these signals, although unlikely, could be that events with a larger charge are made up of several small events fusing simultaneously with the plasma membrane. To examine this possibility, we calculated the probability of observing overlapping fusion events from our records. For this, the latency times between consecutive fusion events during the constant phase of exocytotic activity (between 15 and 150 s of the recording in Figure 4A; mean rate: 4.29 events/s) is constructed. The resulting histogram is well described with a single exponential fit, suggesting that the release process is a Poisson process (Figure 5C). The probability of finding two events within a single measurement period (Colquhoun and Sigworth, 1995) is given by:

$$P_{(\text{time interval} \le t)} = 1 - e^{-t/\tau}.$$

Using the fitted time constant ($\tau = 0.24$ s) we calculated the probability of observing two small events within a time period that equals the mean half-width of a large event ($t = 3110\ \mu s$) as 0.01. This will not change the major characteristics of the frequency distribution and agrees with the visual inspection of the current trace, suggesting that the great majority of the exocytotic events are recorded as discrete signals (Figure 4A). The probability that several vesicles ($\sim$7 small events are needed to mimic the average charge integral of a large event) would fuse so close together is extraordinarily low [$P(t) = 4.8 \cdot 10^{-12}$], suggesting that large events reflect an entity different from small events. As judged from the inflection point (8 fC) in the charge distribution (Figure 5B), we defined small (<8 fC) and large events (>8 fC) as different exocytotic event types reflecting the exocytosis of SSVs and LDCVs, respectively. This distinction holds with a limited accuracy as estimated from the relative areas of the single Gaussian curves (6.5: 1) below 8 fC (Figure 5B, dashed line). The frequen-

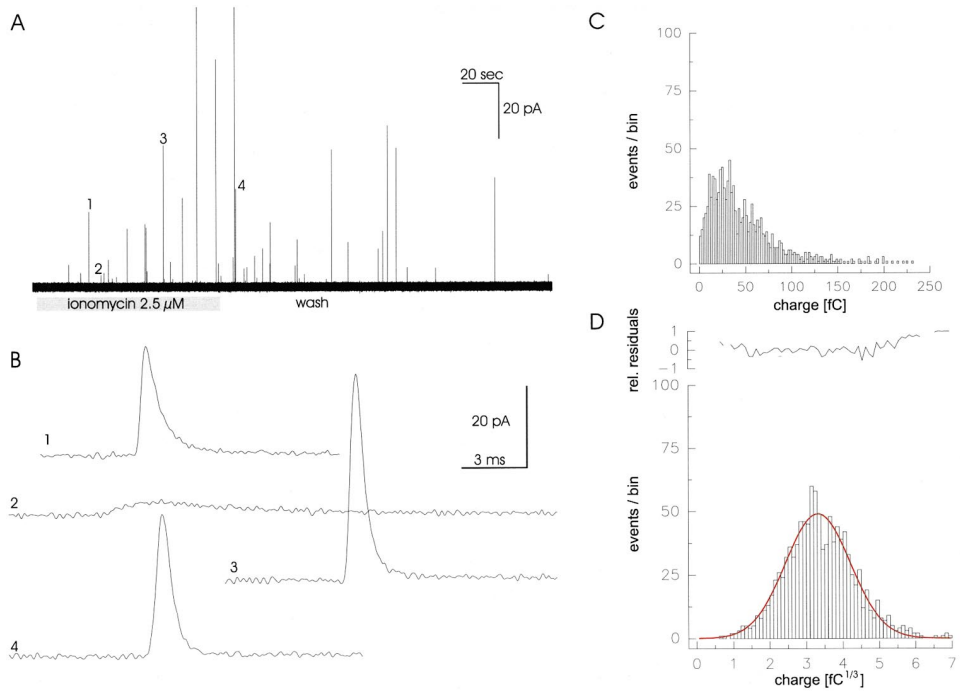

Figure 6. Properties of Amperometric Signals Triggered by Ionomycin Application at Somatic Membranes

(A) Application of ionomycin (2.5 μM, bar) stimulates only the larger event type at somatic membranes. Numbers denote representative events that are shown in (B) on an extended time scale.

(B) The quantal size and the kinetic properties of somatic events (see also Figure 7) suggest that release signals are due to transmitter discharge from LDCVs.

(C) Charge distribution of amperometric signals is unimodal and lacks the peak observed between 2 fC and 4 fC at axonal recording sites (compare Figure 5A). Data were collected from 12 cells (1084 events, 9 cells with two applications of ionomycin).

(D) The distribution of the cube root of amperometric spike charges is approximated with a single Gaussian curve (red curve, mean = 3.3 $fC^{1/3}$, CV = 0.27); relative residuals are plotted on top.

cies of small and large events observed in ionomycin-stimulated neurons show no correlation with each other ($r = 0.01$, $p < 0.05$, $n = 12$). This is in line with our proposal that transmitter release occurring from independent vesicle populations, rather than from a common source, is responsible for the different quantal sizes of the exocytotic signals (Figure 5D).

Quantal Release at Somatic Sites

A direct test of the hypothesis about the distinct nature of the characterized signal classes is provided by the morphological observation that only LDCVs are found in the somata of our neurons. In fact, application of ionomycin stimulates only the large event type at somatic recording sites (Figures 6A and 6B). The charge distribution lacks the peak at about 3 fC seen at axonal recording sites (Figure 6C, $n = 12$; compare with Figure 5A). The cubic root transformation of the integrated current transients reveals a single peak distribution that can be well described with a single Gaussian probability density function (Figure 6D). The mean cubic root charge of somatic events, as deduced from the fit, has a value of 3.32 ± 0.9 $fC^{1/3}$. The larger quantal size of somatic events compared with their axonal counterparts corresponds well with the 1.6-fold larger volume of somatic vesicles. Furthermore, the observed scatter of the event charges is very similar. A similar variation of charges is observed in recordings from individual cells (mean charge: 3.36 ± 0.26 $fC^{1/3}$, mean SD: 0.925 ± 0.11 $fC^{1/3}$ for somatic events, 12 cells). This suggests that intrinsic properties of the LDCV-mediated signaling, rather than experimental inconsistencies, are responsible for the observed variability. Taken together, we observe a distinct pattern of exocytotic signals at axonal and somatic recording sites that parallels the subcellular distribution of SSVs and LDCVs in our neurons.

Kinetic Properties of Transmitter Release from SSVs and LDCVs

For each spike, the 50%–90% rise time, the width at half-height, and the peak amplitude were determined. A comparison of the histograms of these parameters (Figure 7) indicates a strong similarity between the shapes of the large spikes observed at axonal sites and those of somatic events. This result, together with the finding that somatic recordings lack small events, counters the possibility that partial transmitter discharge from LDCVs contributes significantly to the origin of small events. It should be noted that the frequency distribution of small events shows no contribution of events that exhibit particularly slow kinetics that would be expected if this data range (<8 fC) were significantly "contaminated" by charge contribution from fusion events at distant release sites. This result is likely the consequence of a high collection efficiency of the carbon fiber in direct contact with the releasing cell surface, together with the imposed amplitude threshold of 1.5 pA that excludes distant, low-amplitude events from the analysis. The

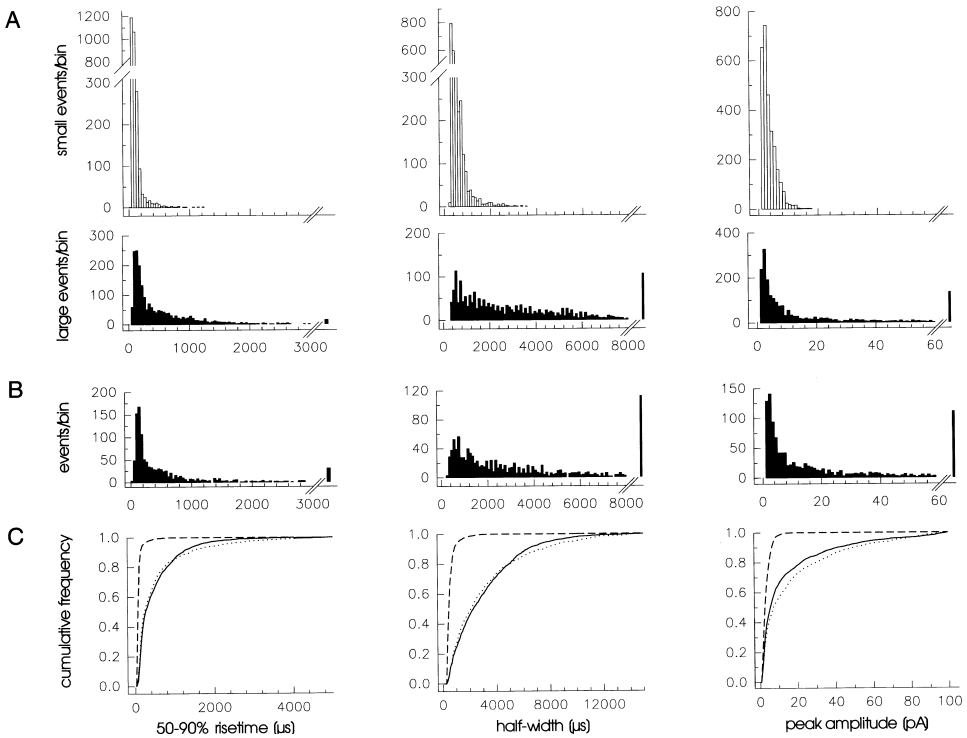

Figure 7. Comparison of Histograms for the Rise Time, Half-Width, and Amplitude of SSV and LDCV Events

(A) Axonal recordings: SSV events (upper row, unfilled bars, 0.2–8.0 fC) differ from LDCV events (lower row, filled bars, 8.0–200 fC) with respect to their rise time, half-width, and peak amplitude (columns 1–3).

(B) Somatic recordings: frequency distribution of the properties of somatic LDCV release signals plotted for the indicated parameters (filled bars, 0.2–300 fC, columns 1–3). The bin width of the histograms is 40 μs, 100 μs, 1 pA for the 50%–90% rise time, half-width, and amplitude, respectively.

(C) Properties of SSV and LDCV release signals, displayed as cumulative frequency distributions for the indicated parameters. SSV events (dashed curve), LDCV (axonal, continuous curve), LDCV (somatic, dotted curve). Note the kinetic properties of LDCV-related events at axonal and somatic recording sites are very similar. Histograms have been normalized. Mean and median values are given in Table 2.

mean values of the parameters for SSV and LDCV exocytosis are given in Table 2. A comparison of the kinetic properties suggests a 5-fold faster transmitter discharge from SSVs than from LDCVs. However, due to the different signal-to-noise ratios, transmitter signals from LDCVs are detectable over further separation distances between the sensor and the exocytotic location than those from SSVs. Thus, it is reasonable to assume that LDCV signals are more susceptible to diffusional distortion. To measure the kinetic properties of release from both vesicle types with similar fidelity, we selected events with rise times faster than 340 μs, comprising about 97% and 53% of the total number of small and large events (>1.5 pA), respectively. About 56% of somatic events are selected by this criterion. A comparison of the median half-width (see Table 2) of such "close" events shows that release signals from LDCVs (1100 μs) are still slower than those from SSVs (440 μs). In fact, <3% of the LDCV events at axonal or somatic sites show a release profile that is similar or faster than the median half-width of SSV events. Thus, properties of the release process are responsible for the observation that the majority of LDCV signals exhibit a main phase of transmitter release ("spike") that is slower than release from SSVs, as will be discussed below.

Charge versus Diameter

Figure 8A plots the mean charge of characterized event types (deduced from the Gaussian fits shown in Figures 5B and 6D) against the mean inner vesicle diameter of the corresponding secretory organelle, assuming an average membrane thickness of 5 nm. When compared on a log/log scale, the combined set of data is fitted with a linear regression that has a slope of 2.8. When "close" events (< 340 μs) are selected, the average cubic root charges obtained from the Gaussian fits of the resulting histograms (data not shown) increase from 2.82 ± 0.81 $fC^{1/3}$ to 3.0 ± 0.9 $fC^{1/3}$ and from 3.31 ± 0.9 $fC^{1/3}$ to 3.49 ± 1.0 $fC^{1/3}$ for LDCV exocytosis at axonal and somatic sites, respectively. No change is seen for SSV signals (values are given in Table 2). A correlation of these data with the vesicle diameters is well described with a linear regression with a slope of 3.0. This result indicates that, on average, the amount of released transmitter is proportional to the volume (r^3) of the secretory organelle. It should be noted that the coefficient of variation (CV = SD/mean) has not decreased when "close" events are selected, suggesting that variations in the amount of transmitter released by the vesicle rather than diffusional loss is the major determinant for the scatter of the event charges in our experiments. The same conclusion is reached with simulations of LDCV release signals by using Monte-Carlo methods (see Appendix for details). Furthermore, LDCV events with rise times ranging from 80 to 340 μs show a similar mean charge (Figure 8B). Thus, the majority of LDCV signals (rise time < 340 μs) is measured with high collection efficiency, providing a reliable estimate of the amount of

Table 2. Properties of Transmitter Release from SSVs and LDCVs

	Axonal Signals		Somatic Signals
	SSV—Small Events	LDCV—Large Events	LDCV—Events
(>1.5 pA)	(0.2–8.0 fC, n = 2793)	(8.0–300 fC, n = 1945)	(0.2–300 fC, n = 1084)
Charge (fC)	2.85 ± 1.4 (2.6)	33.6 ± 24.7 (26.3)	47.4 ± 40.6 (35.8)
Charge ($fC^{1/3}$)	1.36 ± 0.2 (1.37)	2.8 ± 0.8 (2.97)	3.3 ± 0.9 (3.30)
Amplitude (pA)	3.76 ± 2.2 (3.1)	16.1 ± 23 (6.2)	20.0 ± 25 (8.1)
50%–90% risetime (μs)	125 ± 85 (90)	530 ± 566 (280)	580 ± 790 (250)
Half-Width (μs)	615 ± 360 (480)	3110 ± 2700 (2320)	3480 ± 3900 (2200)
Frequency (s^{-1})	1.82 ± 1.45	1.29 ± 1.25	0.42 ± 0.15
(<340 μs)	n = 2716	n = 1035	n = 613
Charge (fC)	2.80 ± 1.3 (2.57)	38.5 ± 27.7 (32.5)	52.30 ± 45 (42.4)
Charge ($fC^{1/3}$)	1.36 ± 0.2 (1.36)	3.0 ± 0.9 (3.19)	3.49 ± 1.0 (3.49)
Amplitude (pA)	3.81 ± 2.2 (3.14)	26.3 ± 27 (15.3)	30.80 ± 29 (19.4)
50%–90% risetime (μs)	110 ± 40 (90)	180 ± 60 (160)	180 ± 65 (160)
Half-Width (μs)	580 ± 270 (440)	1400 ± 1070 (1140)	1390 ± 1140 (1100)

Amperometric signals at axonal sites are classified as SSV- and LDCV-related release signals with a charge smaller or larger than 8 fC, respectively. Events are characterized with respect to area (charge in fC), amplitude (peak value pA), and kinetic parameters. The cubic root charge ($fC^{1/3}$) is deduced from the Gaussian fit of the frequency distribution. The 50%–90% rise time reflects the time span between 50% and 90% amplitude. The half-width gives the duration of the current transient at half-height of its peak amplitude. The frequency refers to the mean secretory rate between 40 and 80 s after the onset of ionomycin application. The lower part of the table refers to values obtained for "close" events with a 50%–90% rise time <340 μs. Data are collected from 12 neurons measured at the axonal tip and from 12 somatic recordings (9 cells stimulated with two applications of ionomycin). Measurements are given as mean ± SD, and numbers in brackets represent median values of the corresponding frequency distribution.

released transmitter. Encouraged by these findings, we compared the individual charge distributions with the size distribution of the corresponding vesicle type. For this, a scale factor was obtained from a plot of the vesicle's cubic root charge against its diameter (Figure 8C). A linear regression with the slope of 1 $fC^{1/3}$/26.45 nm approximates the data. Provided that the majority of stored transmitter molecules is released during exocytotic discharge, this renders an estimate for the average intravesicular serotonin concentration in SSVs and LDCVs of about 270 mM (assuming 4 mols of electrons transferred per mol of serotonin; Bruns and Jahn, 1995). Figures 8D–8F compare the Gaussian fits of the quantal size distributions with the corresponding diameter distributions of the different vesicle types. The variability in quantal size of SSV signals ($charge^{1/3}$) corresponds with the variability of the vesicle's diameter. This suggests that serotonin is stored at a constant intravesicular concentration in SSVs. In contrast, the quantal size of the transmitter signals observed for LDCV exocytosis at both axonal and somatic sites shows a variability that exceeds the variations expected from the size differences of this organelle type.

Discussion

In this study we have characterized the vesicular origin and the quantal variability of transmitter release in serotonergic neurons. As a model system, we used isolated Retzius cells of the leech. Retzius cells are hitherto the only preparation in which exocytosis of SSVs and LDCVs can be simultaneously monitored at the resolution of single vesicles (Bruns and Jahn, 1995). We found that the pattern of exocytotic signals observed at axonal and somatic sites correlates with the subcellular distribution of SSVs and LDCVs, confirming that serotonin is independently released from both types of storage organelles. On average, quantal size varies proportionally to the size differences of SSVs and LDCVs, suggesting that serotonin is stored at similar concentrations in SSVs and LDCVs. Furthermore, our results show that quantal variability of SSV release can be exclusively attributed to the size variability of this class of organelles. These observations indicate that the transmitter concentration within SSVs is maintained at a remarkably constant level and suggest that release from SSVs is an all-or-none event.

Comparing Transmitter Release from SSVs and LDCVs

Electrochemical measurements of transmitter release from neuroendocrine cells and aminergic neurons have shown that unitary amperometric events can be attributed to quantal transmitter discharge from individual vesicles (Wightman et al., 1991; Chow et al., 1992; Alvarez de Toledo et al., 1993; Chen et al., 1994; Zhou and Misler, 1995; Koh and Hille, 1997; Albillos et al., 1998; Jaffe et al., 1998; Pothos et al., 1998). Retzius cells exhibit at distal regions of the axon a large number of morphological specializations that resemble putative release sites and contain mixed populations of SSVs and LDCVs. Whereas LDCVs were shown earlier to contain aminergic transmitter (Kuffler et al., 1987), we have now extended this observation to SSVs by using permanganate fixation. This procedure results in reserpine-sensitive, electron-dense precipitates in SSVs of Retzius cells, consistent with our previous notion that release from both vesicle types contributes to the pattern of amperometric signals at axonal recording sites. SSV exocytosis differs from LDCV exocytosis with respect to frequency and temporal coupling upon stimulation with single action potentials (Bruns and Jahn, 1995). The spatial organization of SSVs within the terminal region occurring often adjacent to presynaptic "thickenings" of the plasma membrane corresponds with the short latency response of small quantal events that occur within the first milliseconds after the action potential, as expected for vesicles that colocalize with the site of transmembrane Ca^{2+} influx. These observations agree with findings in chromaffin cells showing that variable exocytotic delays are best explained by heterogeneous

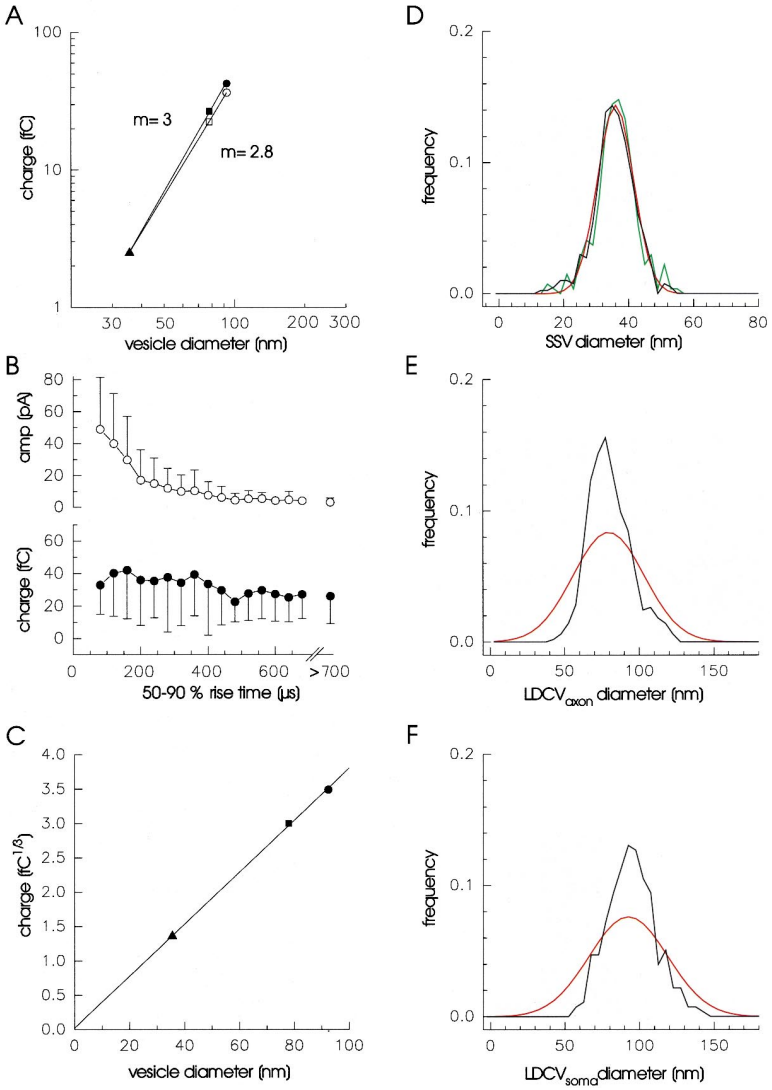

Figure 8. Amperometric Charge versus Vesicular Size

(A) Comparison of the average charge of the event types with the inner vesicle diameter of SSVs (35.7 nm, triangle) and LDCVs (axon, 78.1 nm, square; soma, 93.7 nm, circle). Continuous lines represent linear regressions fitted to the mean values obtained for all events with an amplitude >1.5 pA (slope 2.8, open symbols) or for "close" events with rise times <340 µs (slope 3.0, filled symbols). The correlation supports the view that the released amount of transmitter is proportional to the volume of the organelle.

(B) The charge of axonal LDCV events (>8 fC) does not change for signals with rise times between 80 and 340 µs, whereas the corresponding peak amplitudes decrease with longer rise times. Smaller amplitudes result either from increased separation distances or from mechanisms that hinder transmitter efflux from the organelle. Values are given as mean ± SD.

(C) A scale factor for the charge package of a single vesicle is deduced from the plot of the mean cubic root charge versus the mean inner vesicle diameters (symbols as in [A]). The straight line represents a linear regression fitted to the data, yielding a slope of 1 $fC^{1/3}$/26.45 nm. Amperometric data were taken from events with rise times <340 µs (see Table 2).

(D–F) Comparison of the cube-rooted charge distributions (red curves, Gaussian fits) with the diameter distribution of the corresponding organelle (black curves). Charge distributions are scaled with 26.45 nm/$fC^{1/3}$. Mean values of the diameter distributions are adjusted to the corresponding inner vesicle diameter (given in [A]). Data are taken from events with rise times <340 µs.

(D) The frequency density of SSV charges (CV = 0.15; red curve) compares well with the scatter of SSV diameters (black curve; CV = 0.15). A similar close relationship is obtained with the distribution of SSV diameters (CV = 0.14) determined from serial sections (green curve).

(E) The quantal size of axonal LDCV signals (CV = 0.3) varies more than expected from the size distribution of the organelle (CV = 0.17).

(F) The charge distribution of LDCV signals (CV = 0.27) at somatic membranes exceeds the variations expected from the scatter of radii (CV = 0.17). CV values of diameter distributions refer to the inner vesicle diameter.

separation distances between Ca^{2+} channels and the site of granule fusion (Chow et al., 1994; Klingauf and Neher, 1997; Elhamdani et al., 1998). Still, the involvement of different molecular processes controlling the secretion rate of SSVs and LDCVs cannot be excluded.

In this study, we stimulated exocytosis with the Ca^{2+} ionophore ionomycin. This allowed us to gather a large number of exocytotic events that could be resolved as well-separated amperometric spikes facilitating a comparative analysis of transmitter release from SSVs and LDCVs. As with electrical stimulation, we observed two types of amperometric events that are clearly distinguished by their charge, giving rise to a bimodal frequency distribution. In general, the properties of these signals resemble closely those seen upon action potential stimulation (Bruns and Jahn, 1995). In contrast, only the large event type is observed at somatic membranes where only LDCVs are present. The pattern of amperometric signals at somatic sites compares well with the unimodal charge distributions observed in chromaffin cells, pancreatic cells (Finnegan et al., 1996), and PC12 cells (Chen et al., 1994; Schütz and Bruns, unpublished data), which contain only a single class of aminergic storage organelles. These results suggest that the pattern of amperometric signals evoked by ionomycin mirrors the exocytosis of SSVs and LDCVs.

In mast cells and chromaffin cells, exocytosis starts with the formation of a fusion pore that allows for high release rates of 2.5×10^7 molecules per second, generating a "foot signal" that precedes the main amperometric spike (Alvarez de Toledo et al., 1993; Albillos et al., 1998). Pore expansion coincides with the amperometric spike, but the size of such pores and their influence on the time course of release cannot be accurately determined (Ales et al., 1999). A comparison of the median half-width of SSV and LDCV signals (occurring compara-

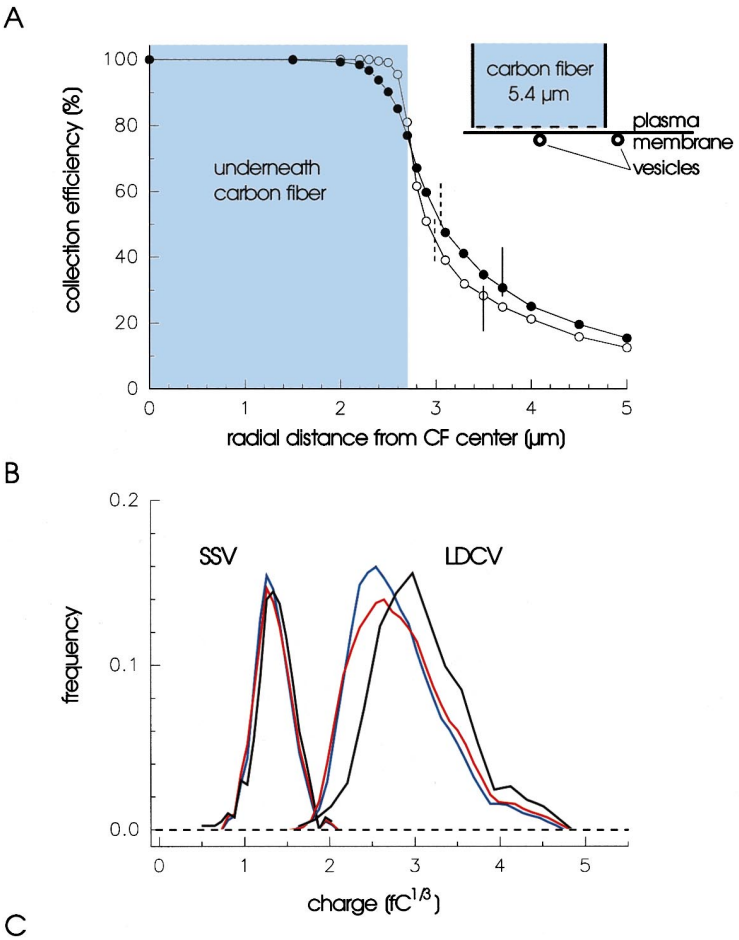

C

template	SSV		LDCV #1		LDCV #2		LDCV #3	
charge$^{1/3}$ [fC]	1.33	(1.36)	2.76	(2.98)	2.66	(2.98)	2.57	(2.98)
diffusional loss [%]	6.5		21.0		29.6		35.8	
amplitude [pA]	6.0	(9.3)	6.2	(9.55)	8.5	(16.3)	17.8	(54)
50-90% risetime [µs]	53	(40)	230	(220)	204	(180)	121	(85)
half width [µs]	275	(190)	2000	(1910)	1260	(1160)	490	(340)

Figure 9. Amperometric Collection Efficiency in the "Cell-Contact" Configuration

(A) Collection efficiency determined by three-dimensional random walk simulations of transmitter release at different radii from the center of the carbon fiber (CF). The fiber tip is placed at an axial distance of 300 nm (filled symbols) and 100 nm (open symbols) from the cell. Detection limits (amplitudes <1.5 pA) for average-sized SSV (2.51 fC; dashed lines) and LDCV signals (27 fC, LDCV #2; continuous lines) are indicated. Inset, see text for explanation.

(B) Calculated charge distributions determined for LDCV (template 1) and SSV release at 300 nm (blue curve) and 100 nm (red curve) cell electrode spacing. Black curves indicate the distribution of charges defined by size variation of the organelles, filled with the same concentration of transmitter.

(C) Properties of simulated amperometric current signals for release from SSVs and LDCVs. Numbers indicate median values of the corresponding frequency distribution (cell electrode spacing, 300 nm). Numbers in brackets indicate properties of the template.

bly close to the detector) reveals a 2.5-fold slower transmitter discharge from LDCVs (1100 µs) than from SSVs (440 µs). Only 3% of LDCV signals exhibit a time course that is similar or faster than the median half-width of the SSV signals. These results suggest that bulk release from LDCVs is hindered. In the case of a rapid expansion of the pore to large diameters, release kinetics might be slowed by restricted diffusivity of 5-HT within an intravesicular storage matrix, as it has been suggested for serotonin release from mast cell vesicles (Alvarez de Toledo et al., 1993; Marszalek et al., 1997). The minimum half-width of such a LDCV fusion event can be estimated by using the simple equation of relationship for one-dimensional diffusion, $t = r^2/2D$, where r is the radius of the vesicle, t is the half-width (approximate time for the mean squared displacement), and D is the diffusion constant. Assuming a 20-fold reduced diffusivity within vesicles ($D_{5HT} = 2.9 \times 10^{-7}$ cm^2 s^{-1}, as has been determined for serotonin release from mast cell vesicles by Marszalek et al., 1997), we estimate a half-width of < 30 µs for LDCV events, an order of magnitude faster than the minimum discharge time observed for this vesicle type (~400 µs). Thus, low diffusivity within a vesicular matrix is unlikely to account for the kinetic differences of SSV and LDCVs release. We propose that dynamics of the expanding fusion pore mainly govern the amperometric spike phase during transmitter discharge from LDCVs.

The different mean quantal sizes observed for SSV and LDCV signals compare well with the average size differences of the organelles suggesting that all types of vesicles store serotonin at a similar concentration (270 mM). Serotonin is transported into vesicles by means of the vesicular monoamine transporter that has been shown to reside on both LDCVs and SSVs (Nirenberg et al., 1995, 1997). Transport depends on the proton electrochemical gradient generated by the vacuolar H^+-ATPase (Maycox et al., 1990; Liu and Edwards,

1997). Our result is in line with the expectation that proton electrochemical gradients across the vesicular membrane of SSVs and LDCVs are similar and that the size of this gradient defines the intravesicular transmitter concentration. An alternative mechanism for the regulation of quantal size has been proposed on the observation that transmitter packaging in secretory organelles is limited by the rate of neurotransmitter uptake (Song et al., 1997; Fon et al., 1997; Travis et al., 2000). These observations have led to the hypothesis that the intravesicular concentration is set by a balance between uptake and leakage from the vesicle (Williams, 1997). Our results do not exclude the possibility that transport activity rather than a transvesicular electrochemical gradient is the limiting factor in serotonin loading, provided that transport activity (e.g., number of transporters per vesicle) and counteracting drain are similar or vary proportionally to each other in the different organelle types. Furthermore, the possibility that vesicular filling is governed by a hitherto unidentified "sensor" mechanism cannot be discarded. Interestingly, recent studies in neuroendocrine cells and serotonergic neurons suggest that trimeric GTPases modulate vesicular transmitter content by regulation of the monoamine transporter (Höltje et al., 2000). The latter mechanism may also be an attractive target of intracellular signaling pathways that regulate quantal size (van der Kloot, 1991; Sulzer and Pothos, 2000).

Quantal Variability

Theoretical and experimental evidence has suggested the potential importance of structural and functional properties of synapses such as vesicle size, the geometry of the synaptic cleft and of the extrajunctional space, as well as binding to neurotransmitter transporters in shaping the transmitter concentration profile in the synaptic cleft (Bruns et al., 1993; Clements, 1996; Frerking and Wilson, 1996; Kleinle et al., 1996; Wahl et al., 1996; Asztely et al., 1997; Diamond and Jahr, 1997; Walmsley et al., 1998). In fact, recent evidence corroborates the view that varying transmitter concentrations in the synaptic cleft and a lack of receptor saturation contribute to quantal variability of GABA mini amplitudes in amacrine cells (Frerking et al., 1995) and of glutamatergic unitary events in hippocampal cultures and slice preparations (Forti et al., 1997; Liu et al., 1999; Choi et al., 2000). Our experiments provide information to what extent presynaptic sources can be responsible for quantal variability. We observed that the amount of transmitter released from a SSV varies proportionally with the volume of the organelle. The close correspondence between the distribution of cube-rooted amperometric charges and the scatter of vesicle radii suggests that all SSVs are indeed filled with the same concentration of serotonin (270 mM). A similar mean value and dispersion of quantal SSV size was observed upon stimulation with single action potentials or hypertonic sucrose solution (unpublished data), suggesting that with a variety of physiologically distinct stimuli, transmitter discharge from SSVs is an all-or-none event. The coefficient of variation of SSV charges (CV = 0.4–0.5, untransformed data) in our neurons compares well with that observed for amplitudes of unitary events at single release sites in hippocampal neurons (Liu et al., 1999). SSVs in these neurons are slightly smaller but exhibit a similar size scatter (Bekkers et al., 1990). If our finding of a constant intravesicular transmitter concentration holds for glutamatergic SSVs, one can speculate that vesicle size determines mainly the variability of quantal glutamate release in hippocampal neurons. This is in line with the observation of Bekkers et al. (1990) reporting a reasonable agreement between the distribution of vesicle radii and the cube-rooted amplitude distribution of unitary glutamatergic events.

In contrast to the results obtained for SSVs, we failed to observe a similarly close relationship between quantal size and the size distribution of LDCVs. We would like to emphasize that LDCV signals generally exhibit a continuous decay of the current signal, giving no indication that incomplete or interrupted transmitter discharge contributes to quantal variability, as one might expect when premature closing of a fusion pore terminates release. This agrees with observations in chromaffin cells showing that even larger-sized chromaffin granules complete their discharge during a kiss-and-run fusion event (Ales et al., 1999). Our random walk simulations (see Appendix for details) suggest that a contribution of "rim events" with reduced charge (due to reduced collection efficiency outside of the electrode contact area) is not sufficient to account for the entire divergence between the frequency distributions, suggesting that serotonin packaging in LDCVs is indeed more variable than in SSVs. The increased quantal variability of LDCV events might be a consequence of the biogenesis of this vesicle type. LDCVs derive from the *trans*-Golgi network, whereas SSVs undergo local recycling within axon terminals. Previous studies suggested that LDCVs undergo a complex process of maturation while they travel to the terminal by axonal flow (Winkler, 1997). We observed that LDCVs in the soma are larger than at axonal sites, suggesting that a reduction in size accompanies maturation. Such a scenario may also interfere with the electrochemical gradient or produce a large diversity in the number of neurotransmitter transporters per vesicle. It remains to be clarified whether sequestration of membrane from LDCVs contributes also to the origin of SSVs in these neurons, a concept that has been controversially discussed (Jahn and de Camilli, 1991; Bauerfeind et al., 1995; Winkler, 1997). Since LDCVs release their content preferentially at extrasynaptic locations, the functional consequences of a variable serotonin loading of LDCVs may not be as crucial as for rapid and discrete synaptic signaling that relies on the exocytosis of SSVs. The ability of LDCVs to store and release large amounts of serotonin make these vesicles prime candidates for the paracrine mode of serotonin action in the CNS.

Experimental Procedures

Animals

Experiments were performed on cells of adult leeches (*Hirudo medicinalis*) kept in laboratory aquaria.

Cell Culture

Retzius cells and AE (annulus erector) motoneurons were isolated from desheathed ganglia by suction pipettes (Dietzel et al., 1986) after enzyme treatment with collagenase-dispase (2 mg/ml for 1 hr; Boehringer Mannheim, Germany) and were kept on nonadhesive culture dishes (Falcon no. 3001) in Leibowitz L-15 medium (GIBCO, Germany) supplemented with 6% fetal calf serum (GIBCO), glucose (4 mg/ml), and gentamycin (0.1 mg/ml; Merk, Germany). A crucial point in the isolation procedure was to ensure that a long stretch of the original process was prepared together with the soma. The

cells were transferred after 24 hr into culture dishes coated with poly-L-ornithine (Sigma, Germany) and filled with Leibowitz medium. After adhesion of the neurons, the medium was supplemented as described above. Under these conditions, the cells did not develop extended neurites and were used for recordings at room temperature (23°C) on days 2–4 of culture.

Electron Microscopy

For electron microscopy, neurons were plated on poly-L-ornithine-coated Petriperm dishes (Bachhofer, Germany). The cells were fixed in 3% glutaraldehyde in 0.1 M cacodylate buffer (pH 7.4) and post-fixed in 2% OsO_4 in 0.1 M cacodylate buffer (pH 7.4) at 4°C for 1 hr. The specimen was contrasted en bloc in 2% uranyl acetate (aqueous) at 4°C for 1 hr and serially dehydrated in ethanol followed by infiltration in Embed-812 (Electron Microscopy Science, München, Germany). The Embed was polymerized at 60°C for 48 hr. The resin containing individual neurons was mounted on a dowel. Ultrathin sections of gray/silver interference color (estimated thickness, 50 nm, cut parallel to the plane of the culture dish) were counterstained with 2% uranyl acetate (aqueous) and lead citrate (0.4 mg/ml [pH 12.0]) and analyzed with a Philips CM 120 (80 kV) electron microscope. Permanganate fixation of cultured neurons was performed according to Hökfelt and Jonsson (1968). Retzius cells and AE motoneurons were fixed in 3% ice-cold sodium permanganate (0.1 M sodium phosphate [pH 7.0]), rinsed in Ringer's solution, contrasted en bloc in 2% uranyl acetate (aqueous) at 4°C for 1 hr, dehydrated, and embedded as described above. Ultrathin sections were cut at silver interference color. The percentage of electrondense SSV profiles was evaluated on prints of 60,000× magnification. Vesicular profiles of SSV size were counted as "dense" when they exhibited an electron-opaque precipitate similar in density to that of LDCVs.

Morphometric Analysis

The diameter of SSVs was measured on micrographs acquired at a magnification of 60,000× and printed to a final magnification of 180,000×. For measurements of LDCV diameters, micrographs were taken at the somatic periphery and distal regions of the axon (taken at 22,000×) and were printed at 110,000×. The microscope was calibrated with a cross-grating replica (2160 lines/mm). Since the shape of some organelles is slightly elliptical, diameters of SSVs and LDCVs were measured generally for perpendicularly oriented long (a) and short (b) axes (measured with an electronic digital caliper [Mitutoyo, Perschman, Berlin, Germany] between the outsides of the outer leaflets). The mean diameter was approximated by $d_{aveg} = (a \times b \times c)^{1/3}$, where $c = (a + b)/2$. All organelles with clearly delineated membranes were counted. The mean diameters obtained from a Gaussian fit of the distribution of vesicle diameters were corrected for section thickness (estimated at 50 nm) by using the theoretical solution given by Parsons et al. (1995). SSV diameters were also determined on micrographs obtained from 8 serial sections of 2 cells and printed at 205,000×. To identify SSV profiles that are entirely enclosed within an 80 nm section, we aligned morphological structures with preceding and following sections using LDCVs profiles as "landmarks."

Electrophysiology

Single-stranded carbon fibers (model, Pan-T650; cross-sectional diameter, 5.4 μm; Amoco Performance Products, Greenville, SC) were polyethylene insulated as described (Chow and von Rüden, 1995), connected to copper wires using conductive carbon paste (Electrodag 5513, Acheson Colloids, Scheemda, Netherlands), and mounted in glass microcapillaries (borosilicate glass, GC150F10, Clark Electromedical Instruments, United Kingdom) with two-component epoxy glue. Amperometric currents were recorded with a List EPC-7 amplifier (Heka Electronics, Lambrecht, Germany; electrode voltage set to +650 mV). The tip of the carbon fiber was cut with a surgical blade just before the experiment to ensure cleanliness and sensitivity of the exposed tip surface. Transsected tips were examined for irregularities at 800× magnification (objective, Olympus ULWD CDPlan 40×) on the stage of a microforge (Narishige, MF-90, Tokyo, Japan) and were recut if the exposed carbon surface was visibly uneven. In all experiments the actual membrane potential was recorded with an additional microelectrode connected to a conventional bridge amplifier. Microelectrodes (borosilicate glass, GC150F10, Clark Electromedical Instruments) were back filled with 3 M potassium acetate and 100 mM KCl and had resistances ranging from 30 to 50 MΩ. The external saline contained (in mM): 130 NaCl, 4 KCl, 1 $CaCl_2$, 48 mM glucose, and 10 HEPES-NaOH (pH 7.3). Experiments were performed on the stage of an inverted microscope (Zeiss Axiovert 100, Oberkochen, Germany). Amperometric currents were filtered at 3 kHz (8-pole, Bessel), digitized gapfree at a rate of 25–50 kHz, and stored on a personal computer. For data collection and evaluation, the programs pClamp6 (Axon Instruments, Foster City, CA) and AutesW (NPI Electronics, Tamm, Germany) were used. Amperometric signals were again digitally filtered at 3 kHz (effective overall filtering 2.1 kHz) and were analyzed with an AutesW-based customized event detection routine (written by Bruns) that uses a threshold criterion of 1.5 pA and allows for direct visual control of the determination of the event's properties. Current transients that exceeded the average baseline noise standard deviation (0.28 ± 0.04 pA) by more than five times were included, a criterion that yields a false event rate of 0.003 events/s, reflecting about one-thousandth of the mean rate of secretory events during ionomycin application (3.1 ± 1.9 events/s). Drugs and external solutions were delivered from a multichannel perfusion pipette (Carbone and Lux, 1987) placed ~340 μm from the cell. Change of superfusion solutions was accomplished by triggered electromagnetic valves (The Lee Co., Westbrook, CT). The slow solution exchange (time constant, 600–800 ms), as determined by tip potential measurements with a microelectrode placed at a distance of 2–10 μm from the cell, will not affect the charge integral of the amperometric signal measured over a time period of 40 ms. Measurements are given as mean ± SD, unless indicated otherwise. Data were fitted using a least squares criterion.

Chemicals

Ionomycin was obtained from Calbiochem (Germany).

Appendix

Amperometry is well suited for quantifying the amount of released transmitter because electroxidative consumption generates steep concentration gradients and thus increases the collection efficiency (Wightman et al., 1995). Still, a quantitative answer depends on spatial arrangement, the relative location of release sites, and the detecting surface (Schroeder et al., 1992; Haller et al., 1998). To minimize diffusional loss of transmitter, the carbon fiber was placed directly on the releasing cell surface as visualized by deformation of the cell membrane. We performed Monte-Carlo simulations to estimate the amperometric collection efficiency in the "cell-contact" configuration and to study whether diffusional loss of transmitter released from a vesicle may contribute to the scatter of charges observed in our experiments. It was assumed that exocytotic events occur in a random and uniform distribution over the cell surface. The carbon fiber (5.4 μm diameter) is placed at an axial distance of 300 nm or 100 nm from the cell membrane to account for variable cell–electrode spacing. Molecules allowed to diffuse into the surrounding medium with a diffusion coefficient of 5.4×10^{-6} cm^2 s^{-1} (Gerhardt and Adams, 1982) were reflected at the cell surface and the cylindrical surface of the fiber (continuous lines, inset, Figure 9) and absorbed at the disc-like tip of the fiber (dashed line). Release sites are distributed at radial distances from the central axis of the carbon fiber ranging from 0 to 5 μm. The probability of release is proportional to the corresponding area of the surface segment. For each release site, an amperometric current signal was calculated by a random walk process with 42,000 molecules. Transmitter molecules were released with a time course determined by a template to mimic properties of noninstantaneous transmitter discharge from LDCVs. Recorded fast current transients (filtered at 5.7 kHz, 8-pole, Bessel) were selected as templates, assuming that such events occur close to the surface of the fiber and thus report faithfully the kinetics of release. Templates with different kinetic properties were compared (Figure 9C). To simulate release from differentially sized LDCVs, amplitude and charge of the template were scaled proportionally to the volume of the organelle, and the frequency of such signals was adjusted to the frequency distribution of LDCV diameters at axonal sites. Events with amplitudes >1.5 pA were analyzed

with respect to charge, amplitude, and kinetic properties; the charge was integrated over a 40 ms time period as for the experimental signals. Median values of the corresponding frequency distributions are given in Figure 9C. We found that peak amplitudes and kinetic properties of the signals predicted from the "rapid-releasing" template (LDCV #3) are incompatible with the experimental data (Figure 9C, compare Table 2). In contrast, a reasonable agreement between simulated and experimental results was obtained for "slow-releasing" templates (LDCV #1 and #2). This is consistent with the observation that properties of the release process are responsible for slow kinetics of transmitter discharge from LDCVs. The calculated distribution of LDCV charges ($charge^{1/3}$; LDCV #1, CV = 0.18; LDCV #2, CV = 0.20) shows a similar scatter as the charge distribution set by the size variability of the vesicles (CV = 0.17; Figure 9B). Even for template LDCV #3, the predicted variation of charges (CV = 0.22) is much smaller than observed in the experiment (CV = 0.3). This confirms the view that variability in the amount of released transmitter rather than diffusional loss determines the scatter of charges in the "cell-contact" configuration. On average, about 21%–29% of the molecules released from LDCVs can escape detection by the carbon fiber. Similar calculations for SSV release (using a fast template with a half-width of 190 μs, amplitude 10.3 pA, charge 2.5 fC) revealed a maximum loss of 6.5% of the discharged molecules. The relative difference of diffusional loss for SSV and LDCV signals (14%–23%) compares well with the experimentally observed increase of LDCV charges (16%–19%) when LDCV events with rise times similar to those of SSV events are selected (≤340 μs; Table 2). Similar collection efficiencies were obtained for an axial distance of 100 nm (Figure 9B). Thus, such variability in axial distance due to irregularities of the carbon fiber tip will not significantly affect the collection efficiency.

Acknowledgments

The authors would like to express their gratitude to Drs. E. Neher, A. Marty, S. Arch, and U. Kuhnt for valuable discussions. We thank S. Bruns-Engers for excellent technical assistance.

Received July 12, 2000; revised August 14, 2000.

References

Albillos, A., Dernick, G., Horstmann, H., Almers, W., Alvarez de Toledo, G., and Lindau, M. (1998). The exocytotic event in chromaffin cells revealed by patch amperometry. Nature *389*, 509–512.

Ales, E., Tabares, L., Poyato, J.M., Valero, V., Lindau, M., and Alvarez de Toledo, G. (1999). High calcium concentrations shift the mode of exocytosis to the kiss-and-run mechanism. Nat. Cell Biol. *1*, 40–44.

Alvarez de Toledo, G., Fernandez-Chacon, R., and Fernandez, J.M. (1993). Release of secretory products during transient vesicle fusion. Nature *363*, 554–558.

Arluison, M., and de la Manche, I.S. (1980). High-resolution radioautographic study of the serotonin innervation of the rat corpus striatum after intraventricular administration of [3H]5-hydroxytryptamine. Neuroscience *5*, 229–240.

Asztely, F., Erdemli, G., and Kullmann, D.M. (1997). Extrasynaptic glutamate spillover in the hippocampus: dependence on temperature and the role of active glutamate uptake. Neuron *18*, 281–293.

Auger, C., and Marty, A. (1997). Heterogeneity of functional synaptic parameters among single release sites. Neuron *19*, 139–150.

Bauerfeind, R., Jelinek, R., Hellwig, A., and Huttner, W.B. (1995). Neurosecretory vesicles can be hybrids of synaptic vesicles and secretory granules. Proc. Natl. Acad. Sci. USA *92*, 7342–7346.

Beaudet, A., and Descarries, L. (1981). The fine structure of central serotonin neurons. J. Physiol. *77*, 193–203.

Bekkers, J.M., Richerson, G.B., and Stevens, C.F. (1990). Origin of variability in quantal size in cultured hippocampal neurons and hippocampal slices. Proc. Natl. Acad. Sci. USA *87*, 5359–5362.

Bruns, D., and Jahn, R. (1995). Real-time measurement of transmitter release from single synaptic vesicles. Nature *377*, 62–65.

Bruns, D., Engert, F., and Lux, H.D. (1993). A fast activating presynaptic reuptake current during serotonergic transmission in identified neurons of Hirudo. Neuron *10*, 559–572.

Carbone, E., and Lux, H.D. (1987). Kinetics and selectivity of a low-voltage-activated calcium current in chick and rat sensory neurones. J. Physiol. (Lond.) *386*, 547–570.

Chazal, G., and Ralston, H.J., III. (1987). Serotonin-containing structures in the nucleus raphe dorsalis of the cat: an ultrastructural analysis of dendrites, presynaptic dendrites, and axon terminals. J. Comp. Neurol. *259*, 317–329.

Chen, T.K., Luo, G., and Ewing, A.G. (1994). Amperometric monitoring of stimulated catecholamine release from rat pheochromocytoma (PC12) cells at the zeptomole level. Anal. Chem. *66*, 3031–3035.

Choi, S., Klingauf, J., and Tsien, R.W. (2000). Postfusional regulation of cleft glutamate concentration during LTP at "silent synapses". Nat. Neurosci. *3*, 330–336.

Chow, R.H., and von Rüden, L. (1995). Electrochemical detection of secretion from single cells. In Single-Channel Recording, Second Edition, B. Sakmann and E. Neher, eds. (New York: Plenum Press), pp. 245–275.

Chow, R.H., von Rüden, L., and Neher, E. (1992). Delay in vesicle fusion revealed by electrochemical monitoring of single secretory events in adrenal chromaffin cells. Nature *356*, 60–63.

Chow, R.H., Klingauf, J., and Neher, E. (1994). Time course of Ca^{2+} concentration triggering exocytosis in neuroendocrine cells. Proc. Natl. Acad. Sci. USA *91*, 12765–12769.

Clements, J.D. (1996). Transmitter timecourse in the synaptic cleft: its role in central synaptic function. Trends Neurosci. *19*, 163–171.

Colquhoun, D., and Sigworth, F.J. (1995). Fitting and statistical analysis of single-channel records. In Single-Channel Recording, Second Edition, B. Sakmann and E. Neher, eds. (New York: Plenum Press), pp. 483–587.

Diamond, J.S., and Jahr, C.E. (1997). Transporters buffer synaptically released glutamate on a submillisecond time scale. J. Neurosci. *17*, 4672–4687.

Dietzel, I.D., and Gottmann, K. (1988). Development of dopamine-containing neurons and dopamine uptake in embryos of Hirudo medicinalis. Dev. Biol. *128*, 277–283.

Dietzel, I.D., Drapeau, P., and Nicholls, J.G. (1986). Voltage dependence of 5-hydroxytryptamine release at a synapse between identified leech neurons in culture. J. Physiol. *372*, 191–205.

Edwards, F.A., Konnerth, A., and Sakmann, B. (1990). Quantal analysis of inhibitory synaptic transmission in the dentate gyrus of rat hippocampal slices: a patch-clamp study. J. Physiol. (Lond.) *430*, 213–249.

Elhamdani, A., Zhou, Z., and Artalejo, C.R. (1998). Timing of dense-core vesicle exocytosis depends on the facilitation L-type Ca channel in adrenal chromaffin cells. J. Neurosci. *18*, 6230–6240.

Finnegan, J.M., Pihel, K., Cahill, P.S., Huang, L., Zerby, S.E., Ewing, A.G., Kennedy, R.T., and Wightman, R.M. (1996). Vesicular quantal size measured by amperometry at chromaffin, mast, pheochromocytoma, and pancreatic beta-cells. J. Neurochem. *66*, 1914–1923.

Fon, E.A., Pothos, E.N., Sun, B.C., Killeen, N., Sulzer, D., and Edwards, R.H. (1997). Vesicular transport regulates monoamine storage and release but is not essential for amphetamine action. Neuron *19*, 1271–1283.

Forti, L., Bossi, M., Bergamaschi, A., Villa, A., and Malgaroli, A. (1997). Loose-patch recordings of single quanta at individual hippocampal synapses. Nature *388*, 874–878.

Frerking, M., and Wilson, M. (1996). Saturation of postsynaptic receptors at central synapses? Curr. Opin. Neurobiol. *6*, 395–403.

Frerking, M., Borges, S., and Wilson, M. (1995). Variation in GABA mini amplitude is the consequence of variation in transmitter concentration. Neuron *15*, 885–895.

Fried, G., Thureson-Klein, A., and Lagercrantz, H. (1981). Noradrenaline content correlated to matrix density in small noradrenergic vesicles from rat seminal ducts. Neuroscience *6*, 787–800.

Gerhardt, G., and Adams, R.N. (1982). Determination of diffusion coefficients by flow injection analysis. Anal. Chem. *54*, 2618–2620.

Haller, M., Heinemann, C., Chow, R.H., Heidelberger, R., and Neher, E. (1998). Comparison of secretory responses as measured by membrane capacitance and by amperometry. Biophys. J. *74*, 2100–2113.

Henderson, L.P. (1983). The role of 5-hydroxytryptamine as a transmitter between identified leech neurones in culture. J. Physiol. (Lond.) *339*, 309–324.

Hökfelt, T. (1968). In vitro studies on central and peripheral monoamine neurons at the ultrastructural level. Z. Zellforsch. *91*, 1–74.

Hökfelt, T., and Jonsson, G. (1968). Studies on reaction and binding of monoamines after fixation and processing for electron microscopy with special reference to fixation with potassium permanganate. Histochemie *16*, 45–67.

Höltje, M., von Jagow, B., Pahner, I., Lautenschlager, M., Hortnagl, H., Nurnberg, B., Jahn, R., and Ahnert-Hilger, G. (2000). The neuronal monoamine transporter VMAT2 is regulated by the trimeric GTPase Go(2). J. Neurosci. *20*, 2131–2141.

Jaffe, E.H., Marty, A., Schulte, A., and Chow, R.H. (1998). Extrasynaptic vesicular transmitter release from the somata of substantia nigra neurons in rat midbrain slices. J. Neurosci. *18*, 3548–3553.

Jahn, R., and de Camilli, P. (1991). Membrane proteins of synaptic vesicles: markers for neurons and neuroendocrine cells: tools for the study of neurosecretion. In Markers for Neural and Endocrine Cells, M. Gratzl and K. Langley, eds. (New York: VCH), pp. 25–92.

Klein, R.L., Lagercrantz, H., and Zimmermann, H. (1982). Ultrastructural preservation of vesicles in sympathetic nervous tissue. In Neurotransmitter Vesicles (London: Academic Press), pp. 65–87.

Kleinle, J., Vogt, K., Luscher, H.R., Muller, L., Senn, W., Wyler, K., and Streit, J. (1996). Transmitter concentration profiles in the synaptic cleft: an analytical model of release and diffusion. Biophys. J. *71*, 2413–2426.

Klingauf, J., and Neher, E. (1997). Modeling buffered Ca2+ diffusion near the membrane: implications for secretion in neuroendocrine cells. Biophys. J. *72*, 674–690.

Koh, D.S., and Hille, B. (1997). Modulation by neurotransmitters of catecholamine secretion from sympathetic ganglion neurons detected by amperometry. Proc. Natl. Acad. Sci. USA *94*, 1506–1511.

Korn, H., and Faber, D.S. (1991). Quantal analysis and synaptic efficacy in the CNS. Trends Neurosci. *14*, 439–445.

Kuffler, D.P., Nicholls, J., and Drapeau, P. (1987). Transmitter localization and vesicle turnover at a serotoninergic synapse between identified leech neurons in culture. J. Comp. Neurol. *256*, 516–526.

Lagnado, L., Gomis, A., and Job, C. (1996). Continuous vesicle cycling in the synaptic terminal of retinal bipolar cells. Neuron *17*, 957–967.

Lent, C.M., Ono, J., Keyser, K.T., and Karten, H.J. (1979). Identification of serotonin within vital-stained neurons from leech ganglia. J. Neurochem. *32*, 1559–1563.

Lenzi, D., Runyeon, J.W., Crum, J., Ellisman, M.H., and Roberts, W.M. (1999). Synaptic vesicle populations in saccular hair cells reconstructed by electron tomography. J. Neurosci. *19*, 119–132.

Liu, Y., and Edwards, R.H. (1997). The role of vesicular transport proteins in synaptic transmission and neural degeneration. Annu. Rev. Neurosci. *20*, 125–156.

Liu, G., Choi, S., and Tsien, R.W. (1999). Variability of neurotransmitter concentration and nonsaturation of postsynaptic AMPA receptors at synapses in hippocampal cultures and slices. Neuron *22*, 395–409.

Marszalek, P.E., Farrell, B., Verdugo, P., and Fernandez, J.M. (1997). Kinetics of release of serotonin from isolated secretory granules. II. Ion exchange determines the diffusivity of serotonin. Biophys. J. *73*, 1169–1183.

Maycox, P.R., Hell, J.W., and Jahn, R. (1990). Amino acid neurotransmission: spotlight on synaptic vesicles. Trends Neurosci. *13*, 83–87.

McAdoo, D.J., and Coggeshall, R.E. (1976). Gas chromatographic-mass spectrometric analysis of biogenic amines in identified neurons and tissues of Hirudo medicinalis. J. Neurochem. *26*, 163–167.

Moukhles, H., Bosler, O., Bolam, J.P., Vallee, A., Umbriaco, D., Geffard, M., and Doucet, G. (1997). Quantitative and morphometric data indicate precise cellular interactions between serotonin terminals and postsynaptic targets in rat substantia nigra. Neuroscience *76*, 1159–1171.

Nirenberg, M.J., Liu, Y., Peter, D., Edwards, R.H., and Pickel, V.M. (1995). The vesicular monoamine transporter 2 is present in small synaptic vesicles and preferentially localizes to large dense core vesicles in rat solitary tract nuclei. Proc. Natl. Acad. Sci. USA *92*, 8773–8777.

Nirenberg, M.J., Chan, J., Liu, Y., Edwards, R.H., and Pickel, V.M. (1997). Vesicular monoamine transporter-2: immunogold localization in striatal axons and terminals. Synapse *26*, 194–198.

Palay, S.L., and Chan-Palay, V. (1974). The mossy fiber. In Cerebellar Cortex: Cytology and Organization (Springer: New York), p. 159.

Parsons, T.D., Coorssen, J.R., Horstmann, H., and Almers, W. (1995). Docked granules, the exocytic burst, and the need for ATP hydrolysis in endocrine cells. Neuron *15*, 1085–1096.

Plattner, H., Artalejo, A.R., and Neher, E. (1997). Ultrastructural organization of bovine chromaffin cell cortex-analysis by cryofixation and morphometry of aspects pertinent to exocytosis. J. Cell Biol. *139*, 1709–1717.

Pothos, E.N., Davila, V., and Sulzer, D. (1998). Presynaptic recording of quanta from midbrain dopamine neurons and modulation of the quantal size. J. Neurosci. *18*, 4106–4118.

Raastad, M., Storm, J.F., and Anderson, P. (1992). Putative single quantum and single fibre excitatory postsynaptic currents show similar amplitude range and variability in rat hippocampal slices. Eur. J. Neurosci. *4*, 113–117.

Redman, S. (1990). Quantal analysis of synaptic potentials in neurons of the central nervous system. Physiol. Rev. *70*, 165–198.

Rude, S., Coggeshall, E., and Van Orden, L.S., III. (1969). Chemical and ultrastructural identification of 5-hydroxytryptamine in an identified neuron. J. Cell. Biol. *41*, 832–854.

Sargent, P.B. (1977). Synthesis of acetylcholine by excitatory motoneurons in central nervous system of the leech. J. Neurophysiol. *40*, 453–460.

Schroeder, T.J., Jankowski, J.A., Kawagoe, K.T., Wightman, R.M., Lefrou, C., and Amatore, C. (1992). Analysis of diffusional broadening of vesicular packets of catecholamines released from biological cells during exocytosis. Anal. Chem. *64*, 3077–3083.

Silver, R.A., Cull-Candy, S.G., and Takahashi, T. (1996). Non-NMDA glutamate receptor occupancy and open probability at a rat cerebellar synapse with single and multiple release sites. J. Physiol. (Lond.) *494*, 231–250.

Song, H., Ming, G., Fon, E., Bellocchio, E., Edwards, R.H., and Poo, M. (1997). Expression of a putative vesicular acetylcholine transporter facilitates quantal transmitter packaging. Neuron *18*, 815–826.

Stevens, C.F. (1993). Quantal release of neurotransmitter and long-term potentiation. Cell *72* (*suppl.*), 55–63.

Sulzer, D., and Pothos, E.N. (2000). Regulation of quantal size by presynaptic mechanisms. Rev. Neurosci. *11*, 159–212.

Tang, C.M., Margulis, M., Shi, Q.Y., and Fielding, A. (1994). Saturation of postsynaptic glutamate receptors after quantal release of transmitter. Neuron *13*, 1385–1393.

Thureson-Klein, A. (1983). Exocytosis from large and small dense cored vesicles in noradrenergic nerve terminals. Neuroscience *10*, 245–259.

Till, R., and Banks, P. (1976). Pharmacological and ultrastructural studies on the electron dense cores of the vesicles that accumulate in noradrenergic axons constricted in vitro. Neuroscience *1*, 49–55.

Tong, G., and Jahr, C.E. (1994). Multivesicular release from excitatory synapses of cultured hippocampal neurons. Neuron *12*, 51–59.

Torre, J.C., and Surgeon, J.W. (1976). A methodological approach to rapid and sensitive monoamine histofluorescence using a modified glyoxylic acid technique: the SPG method. Histochemistry *49*, 81–93.

Tranzer, J.P., and Thoenen, H. (1967). Significance of "empty" vesicles in postganglionic sympathetic nerve terminals. Experientia *23*, 123–124.

Travis, E.R., Wang, Y.M., Michael, D.J., Caron, M.G., and Wightman, R.M. (2000). Differential quantal release of histamine and 5-hydroxytryptamine from mast cells of vesicular monoamine transporter 2 knockout mice. Proc. Natl. Acad. Sci. USA *97*, 162–167.

Van der Kloot, W. (1991). The regulation of quantal size. Prog. Neurobiol. *36*, 93–130.

Wahl, L.M., Pouzat, C., and Stratford, K.J. (1996). Monte Carlo simulation of fast excitatory synaptic transmission at a hippocampal synapse. J. Neurophysiol. *75*, 597–608.

Walmsley, B., Alvarez, F.J., and Fyffe, R.E. (1998). Diversity of structure and function at mammalian central synapses. Trends Neurosci. *21*, 81–88.

Wightman, R.M., Jankowski, J.A., Kennedy, R.T., Kawagoe, K.T., Schroeder, T.J., Leszczyszyn, D.J., Near, J.A., Diliberto, E.J., Jr., and Viveros, O.H. (1991). Temporally resolved catecholamine spikes correspond to single vesicle release from individual chromaffin cells. Proc. Natl. Acad. Sci. USA *88*, 10754–10758.

Wightman, R.M., Schroeder, T.J., Finnegan, J.M., Ciolkowski, E.L., and Pihel, K. (1995). Time course of release of catecholamines from individual vesicles during exocytosis at adrenal medullary cells. Biophys. J. *68*, 383–390.

Williams, J. (1997). How does a vesicle know it is full? Neuron *18*, 683–686.

Winkler, H. (1997). Membrane composition of adrenergic large and small dense cored vesicles and of synaptic vesicles: consequences for their biogenesis. Neurochem. Res. *22*, 921–932.

Zhang, B., Koh, Y.H., Beckstead, R.B., Budnik, V., Ganetzky, B., and Bellen, H.J. (1998). Synaptic vesicle size and number are regulated by a clathrin adaptor protein required for endocytosis. Neuron *21*, 1465–1475.

Zhou, Z., and Misler, S. (1995). Amperometric detection of stimulus-induced quantal release of catecholamines from cultured superior cervical ganglion neurons. Proc. Natl. Acad. Sci. USA *92*, 6938–6942.